Photochemistry and Photobiology, 2004, 79(5): 440–446

The Complex of Apomyoglobin with the Fluorescent Dye Coumarin 153¶

P. K. Chowdhury[1], M. Halder[1], L. Sanders[1], R. A. Arnold[1], Y. Liu[1], D. W. Armstrong[1], S. Kundu[2], M. S. Hargrove[2], X. Song[1] and J. W. Petrich*[1]

[1]Department of Chemistry, Iowa State University, Ames, IA and
[2]Department of Biochemistry, Molecular Biology, and Biophysics, Iowa State University, Ames, IA

Received 3 December 2003; accepted 12 February 2004

ABSTRACT

Understanding a protein's dielectric response requires both a theoretical model and a well-defined experimental system. The former has already been proposed by Song (*J. Chem. Phys.* 116, 9359 [2002]). We suggest that the latter is provided by the complex of coumarin 153 (C153) with apomyoglobin (ApoMb). C153 has been exhaustively studied and has proven to be an excellent probe of the solvation dynamics of polar solvents. Myoglobin is one of the most thoroughly studied proteins. Myoglobins from a wide range of species have been subject to X-ray structural analysis and site-directed mutagenesis. Here, we demonstrate the existence of a robust C153–apomyoglobin system by means of molecular dynamics simulations, equilibrium binding studies using a Job's plot and capillary electrophoresis, circular dichroism and time-resolved fluorescence. The reorganization energy of C153 bound to ApoMb is compared with that of C153 in bulk solvent using the method of Jordanides *et al.* (*J. Phys. Chem. B* 103, 7995 [1999]).

INTRODUCTION

In the past decade it has been well established by numerous experimental and theoretical studies that solvation dynamics in polar solvents can be described by linear response theory (1–10). In general, the full frequency-dependent dielectric function of the polar solvent gives a good description of the solvation dynamics from the ultrafast regime to that of diffusive relaxation. Some direct comparisons between theory and experiments have been established (11–14). The success is largely attributable to the dielectric fluctuations of polar solvents being described accurately by simple linear response models such as the dielectric continuum model (14–16). On the other hand, the dielectric response in proteins is more complicated. There exist many length scales owing to the structural constraints created by the carbon backbone. Some studies indicate that a linear response model may be valid from atomistic simulations (17,18). A simple dielectric continuum description of the protein is clearly insufficient, even though such a description has been widely used to correlate experimental data (19–22). A full atomistic description is very time-consuming for large proteins and may also hinder the distillation of transparent physical pictures (23,24).

We have previously proposed to seek a physically well-defined middle ground between the continuum and a full atomistic description of the protein's dielectric response to develop a new model that recognizes the highly inhomogeneous nature of a protein and at the same time avoids the enormous computational cost of atomistic model simulations. To this end, we proposed a collection of structurally constrained polarizable dipoles embedded in a dielectric continuum solvent to describe the dielectric response of a protein. Other models of solvents can also be used provided that the response function of the solvent can be obtained from other sources. The main assumption of our model is the existence of a set of frequency-dependent polarizabilities for each residue, portable to all proteins in nature. The polarizabilities can be obtained by performing detailed molecular dynamics (MD) simulations for small proteins or by solvation dynamics measurements with various mutations. The dielectric response of large proteins can be computed from these intrinsic parameters. Each dipole is located on the center of mass of a residue, and for each such residue there is a frequency-dependent polarizability $\alpha(\omega)$ (in general, a complex quantity such as the dielectric constant function). The total number of polarizable dipoles is thus equal to the total number of residues, and their positions are completely specified by the native structure of the protein.

Studies of the solvation dynamics of proteins offer a powerful means to test the validity of models of their dielectric response. In spite of considerable efforts toward the understanding of the dielectric relaxation processes in proteins (25–28), up to now a reliable estimate for the dielectric response function of proteins is still lacking. Early studies indicated that a slow relaxation ($\sim$1 ns), indeed, exists in myoglobin (29,30) in contrast to the polar solvents. This is not unexpected because of the structural constraints. But the role of a protein's interior motions in its dielectric relaxation is presently unclear from various experimental studies of solvation dynamics in protein environments. Homoelle *et al.* have suggested that the dynamical fluctuations observed in phycobiliproteins involve substantial interior motions of the protein (31). Fraga and Loppnow (32) have shown that the resonance Raman spectra are affected by the different residue compositions of the blue copper proteins from different species. On the other hand, other experimental and theoretical studies of lysozyme seem to suggest that the major contribution of the observed dynamical fluctuations comes from the surrounding water

¶Posted on the website on 27 February 2004
*To whom correspondence should be addressed: Department of Chemistry, Iowa State University, Ames, IA 50011, USA. Fax: 515-294-0105; e-mail: jwp@iastate.edu
Abbreviations: ApoMb, apomyoglobin; CD, circular dichroism; CE, capillary electrophoresis; C153, coumarin 153; DMSO, dimethyl sulfoxide; LIF, laser-induced fluorescence; MD, molecular dynamics.

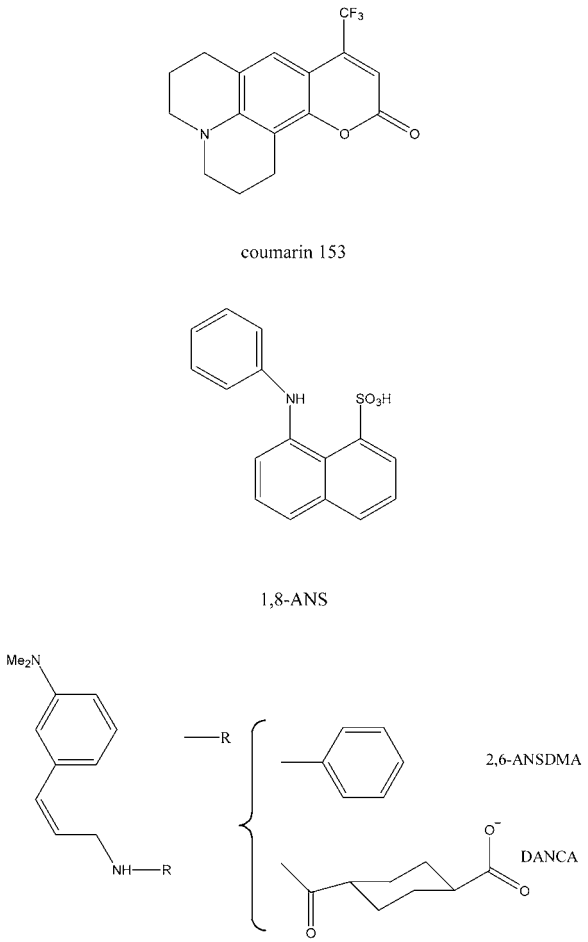

Figure 1. Some fluorescent probes.

solvent and the water molecules attached to the protein surface (33).

Zewail and coworkers used tryptophan fluorescence to study solvation dynamics in proteins. The solvation dynamics were significantly slower for the surface tryptophan residues in subtilisin *Carlsberg* and in monellin than for tryptophan in bulk water. They argued that the slow relaxation is due to the water molecules constrained on the protein surface (27,34,35). Given, however, the $\sim$500 cm^{-1} difference in the reorganization energies for the surface tryptophans in the two proteins, it seems that there is also a considerable relaxation arising from the different amino acids neighboring the tryptophans.

These differences in the interpretations of various experiments are in no small part due to the lack of a reliable dielectric response function for the studied proteins from either experiments or computer simulations. The knowledge of the protein dielectric response provided by our model could shed light on this because it presents a residue-level dielectric response function of proteins. What is also required, however, is a well-characterized experimental system that facilitates the interpretation of the data. To this end, we propose the complex of coumarin 153 (C153) and apomyoglobin (ApoMb). There are three main considerations for the choice of this system. First, coumarins in general, and C153 in particular, are well-characterized and widely used chromophores for solvation dynamics studies (36–46). Second, we can produce a broad range of mutant proteins (47,48) in which one or several amino acids are strategically replaced, so as to test our theoretical model. Third, the structures of many myoglobins and their mutants have been determined to high resolution (49,50). We consequently propose that a fruitful system for studying the protein dielectric response is myoglobin in which the heme has been replaced by C153. The availability of mutant proteins with amino acid replacements near the heme-binding site will eventually permit a quantitative evaluation of local contributions of specific residues to the solvation dynamics of proteins.

Previous attempts to exploit the myoglobin system to study the solvation response of proteins have been made (29,30) using the fluorescent probes 2,6-ANSDMA and DANCA, respectively (Fig. 1). The former probe molecule afforded a single-exponential response of 9.1 ns and the latter, a more complicated response with both shorter and longer response times. The discrepancy between the results for these two probe molecules as well as the predominance of the long-lived response time caused us to search for other probes. We thus initially considered the probe molecules 1,8-ANS and biliverdin, for both of which there are structures of their complexes with ApoMb (51,52). Neither of these chromophores is, however, ideal because their absorption spectra are complicated by overlapping electronic states. Even if internal conversion from higher-lying states to the lower fluorescent state is faster than solvation dynamics, as has been suggested to be the case in tryptophan (27,34,35,53), an accurate determination of the reorganization energy based on the steady-state spectra becomes very difficult. We consequently opted for C153, which not only has been studied in a very wide range of solvents and in the gas phase, but whose excited-state solvation has been demonstrated not to involve any contributions other than those from S_1 (38). Hochstrasser and coworkers have studied the solvation of coumarin 343 in calmodulin (41). These workers attached coumarin 343 to the N-terminus of a tridecapeptide, which was designed to bind tightly to calmodulin. In this system solvation is complete in 100 ps.

MATERIALS AND METHODS

C153 was purchased from Exciton Inc. (Dayton, OH) and used without further purification. ApoMb was prepared using the procedure described elsewhere (54). C153 has low solubility in water. Consequently, addition of apoprotein providing sufficient time for equilibration (45 min) ensured that it was taken up by complex formation. To obtain complexes with different C153–ApoMb ratios, increasing amounts of C153 were added to a 5×10^{-5} *M* protein solution. The C153 solution was prepared by adding microliter amounts of a concentrated stock solution of C153 in methanol to water and sonicating for $\sim$1 h in the dark to ensure complete homogenization of the resulting solution. All the samples were then allowed to equilibrate for 45 min before the steady-state and time-resolved measurements. Completion of equilibration was checked by recording the steady-state spectra at 10-min intervals after the addition of C153 until no change in Stokes shift was observed.

Binding constant measurements, fluorescence. Two stock solutions were prepared of equal concentration, 5×10^{-5} *M,* of ApoMb and C153. From these stock solutions seven 200 μL samples were prepared with an increasing mole fraction, X, of coumarin: 0.1, 0.2, 0.25, 0.5, 0.75, 0.8, and 0.9. After the samples were allowed to stand for approximately 45 min to ensure complete equilibriation, fluorescence intensities were measured and plotted against the mole fraction of coumarin, X, to verify that the maximum intensity occurred at a mole fraction of 0.5, indicating a one-to-one binding stoichiometry. (C153 has very low solubility in water, and the protein ApoMb by itself has no measurable fluorescence in the region where the complex emits. Thus, the fluorescence is directly proportional to the concentration of the protein–coumarin complex.) Using this maximum intensity and the intensity at one other mole fraction, the binding constant, K_B, can be determined (55), where $K_B = (I \times I_0)/(I_0 - I)(I_0[\text{ApoMb}]_T - I[\text{C153}]_T)$. I_0 is the maximum fluorescence intensity at X = 0.5. I is the fluorescence intensity at a given mole fraction, X. $[\text{ApoMb}]_T$ = total concentration of ApoMb at a given X, and the subscript T refers to the total concentration. $[\text{C153}]_T$ is the

concentration of C153 at a given X. The dissociation constant for the complex is $K_D = 1/K_B$.

Binding constant measurements, capillary electrophoresis. Frontal analysis capillary electrophoresis (CE) experiments were performed on a Beckman Coulter P/ACE MDQ CE system equipped with a 488 nm laser-induced fluorescence (LIF) detector. Untreated fused-silica capillaries with 50 μm inner diameter and 360 μm outer diameter were purchased from Polymicro Technologies, Inc. (Phoenix, AZ). The capillaries were 30 cm in length (20 cm to detection window). When a capillary was first used, it was rinsed for 1 min with water, 5 min with 1 *M* NaOH, and 1 min with water. Before each injection the capillary was washed for 0.5 min with water, 0.5 min with 1 *M* NaOH, and 0.5 min with water, followed by 2 min with running buffer. The premixed coumarin–apomyglobin samples were injected at 0.5 psi for 40 s into the capillary. Experiments were performed at 10 kV and a temperature of 25°C. Sample emission was monitored at 520 nm. Data were collected by P/ACE system MDQ software. Sodium phosphate and phosphoric acid were purchased from Fisher Scientifics (Fair Lawn, NJ). Sodium-phosphate buffer (0.2 *M*) at pH 9.0 was used. The phosphate buffer was filtered through 0.22 mm nonpyrogenic filter (Costar Corp., Corming, NY). In the frontal analysis technique C153 and apomyglobin were premixed and injected as a large sample plug onto the capillary column. At pH 9 the apomyglobin is negatively charged. The electrophoretic mobility of the free C153 is different from the mobility of the protein and the protein–coumarin complex. After injection of the large mixed-sample plug, the free coumarin will migrate away from the protein. Equilibrium is maintained where the zones temporarily overlap. The equilibrium-free coumarin concentration is calculated from the height of the resulting plateau. The height of the free coumarin plateau decreases with the addition of apomyglobin because of its binding to coumarin. The plateau height at [ApoMb] = 0 μ*M* was used as the coumarin standard. In this assay a series of sample mixtures with a fixed protein concentration and increasing coumarin concentrations are injected. Performing such experiments at different coumarin concentrations allows the determination of binding constant according to the following equation: $r/(1-r) = nK_B[C153]_f$, where r is the fraction of bound chromophore, n is the number of binding sites, $[C153]_f$ is the free-chromophore concentration in the running buffer, and K_B is the binding constant between ApoMb and C153.

Steady-state spectroscopies. Steady-state absorption spectra were recorded on a Perkin–Elmer Lambda-18 double-beam UV–visible spectrophotometer with 1 nm resolution. The concentration of the apoprotein was determined by monitoring the absorbance at 280 nm, where the molar extinction coefficient is 15.2 mM^{-1} cm^{-1}. Steady-state fluorescence spectra (both excitation and emission) were obtained on a SPEX Fluoromax with a 4 nm band pass and corrected for detector response. For both fluorescence and absorption measurements of the complex, a 3 mm path length quartz cuvette was used. Steady-state circular dichroism (CD) spectra were performed on a JASCO CD spectrometer (J-710). A 3 mm path length cell was also used for these measurements. The concentration of the samples was kept close to micromolar range to avoid saturation of the detector. The data so presented are an average of three scans and were collected at an interval of 1 nm.

Time-resolved spectroscopies. The laser source for the time-correlated single-photon counting measurements was a home-made mode-locked Ti–sapphire laser, tunable from 780 to 900 nm with a repetition rate of 82 MHz. The fundamental from the Ti–sapphire oscillator was modulated by a Pockels cell (Model 360-80, Conoptics Inc., Danbury, CT) to reduce the repetition rate to about 8.8 MHz and was subsequently frequency doubled by focusing tightly into a 0.4 mm beta barium borate crystal. The blue light, which had a central wavelength of 425 nm, provided the excitation source. Emission from the samples of the complex was collected at $\lambda_{em} > 550$ nm with a band-pass filter to reduce the contribution of scattered excitation light interfering with the sample fluorescence. The fluorescence lifetime decays were collected at the magic angle (polarization of 54.7° with respect to the vertical). A half-wave plate was used before the excitation polarizer to ensure vertical polarization of the excitation light. To obtain the rotational dynamics, emission from the samples was collected parallel and perpendicular to the direction of polarization of the excitation pulse. The instrument response function of the apparatus had a full width at half-maximum of 80 ps. The fluorescence lifetime decays were typically collected up to a maximum of 10 000 counts in the peak channel of the multichannel analyzer, whereas for the anisotropy decays the corresponding maximum value was 12 000 counts. Sample integrity was checked by monitoring the excitation and emission spectra before and after the measurements. The coumarin concentration was kept at $\sim 5 \times 10^{-6}$ *M* throughout. A 3 mm cell path length was used for the time-resolved measurements of the complex.

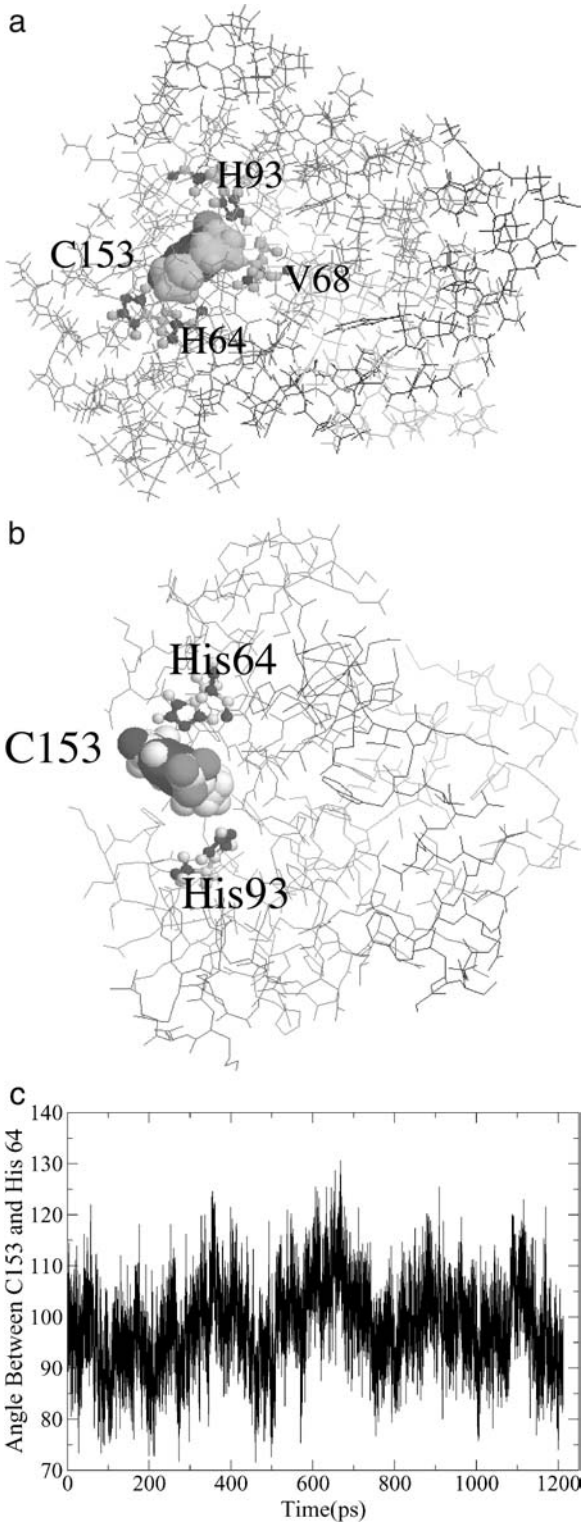

Figure 2. Snapshot of equilibrated C153–ApoMb in water from 3 ns MD simulations using the Amber95 force field: sperm whale ApoMb (a) and horse heart ApoMb (b). The C153 is shown in the space-filling models. Key histidine residues in the heme pocket are also shown. Residue Val68 (one of the residues in contact with C153 in the hydrophobic heme pocket with small nuclear polarizability) is used in one of our mutations (47,48). (c): The time dependence of the relative orientation of C153 with respect to His 93 (see text) from the MD trajectory of the horse heart ApoMb–C153 complex.

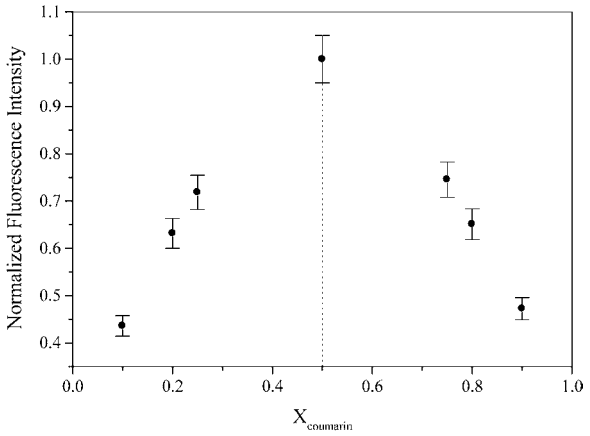

Figure 3. Job's plot for the complexation of C153 with ApoMb. That the fluorescence intensity peaks at a mole fraction value of 0.5 (dotted lines) for C153 is a clear indication of a 1:1 complex formed between the probe molecule and the protein. The data presented are an average of four measurements. The calculated dissociation constant for the complex is 5.65 ± 0.25 μ*M*.

MD simulations. The starting configuration of horse heart myoglobin is from the Protein Data Bank (PDB ID 1WLA) with TIP3P water models. Standard constant pressure–temperature MD was performed using the ORAC package with the Amber force field (56). In all simulations short-range nonbonded interactions were calculated up to a 10 Å cutoff, whereas long-range electrostatic interactions were treated by the smoothed particle mean ewald (SPME) method using a very fine grid, 128 points per axis, with periodic boundary conditions, and Ewald convergence parameter of 0.43 $Å^{-1}$. Three different Nosé–Hoover thermostats were coupled to solute, solvent and total center of mass. An external pressure of 0.1 MPa was applied all along the trajectory. A five–time-step rRESPA (57) algorithm with times of 0.5–1.0–2.0–4.0–12.0 fs was used with bond constraints on hydrogen covalent bonds handled by a Shake-Rattle–like algorithm. The final system was first equilibrated with velocity rescaling for 60 ps at 50 K and 80 ps at 300 K. After this initial equilibration we ran the system for 1 additional ns at constant temperature (T = 300 K) and pressure (P = 0.1 Mpa). To achieve full relaxation the simulation box was entirely flexible for the first 300 ps, whereas for the remainder of the run, only isotropic changes of the box were allowed (58). Finally, the system was simulated for an additional 10 ns. In Fig. 2 are shown snapshots at around 3 ns for the horse heart and the sperm whale ApoMb complexes. One might object that the way to find the equilibrium configuration is to raise the temperature and then to cool the system. This is not recommended. Raising the temperature will most likely denature the protein, and the heme pocket may adopt some highly unlikely conformations that would not be present in the native structure. Because the insertion of C153 in our experiments is done with the native myoglobin structure, the method we use is physically reasonable.

RESULTS AND DISCUSSION

The binding of C153 to ApoMb has been characterized by MD simulations (which predict tight, stable binding in the heme pocket), measurement of its dissociation constant using two different methods, CD (which demonstrates no changes in secondary structure for the complex with respect to that of the native holo protein), and its reorientation time using measurements of the polarized fluorescence decay.

A 10 ns MD simulation using the Amber force field indicates that C153 is stable in the heme pocket and an equilibrium configuration is found (Fig. 2a,b). Also shown in Fig. 2c is a trajectory of the angle between C153 and His 64, which is defined by the vector from N to ester O of C153 and the vector of two Ns on the His 64 side chain. This angle is averaged at 98° with a standard deviation of 8°. Similar results are obtained for the angle between C153 and His 93.

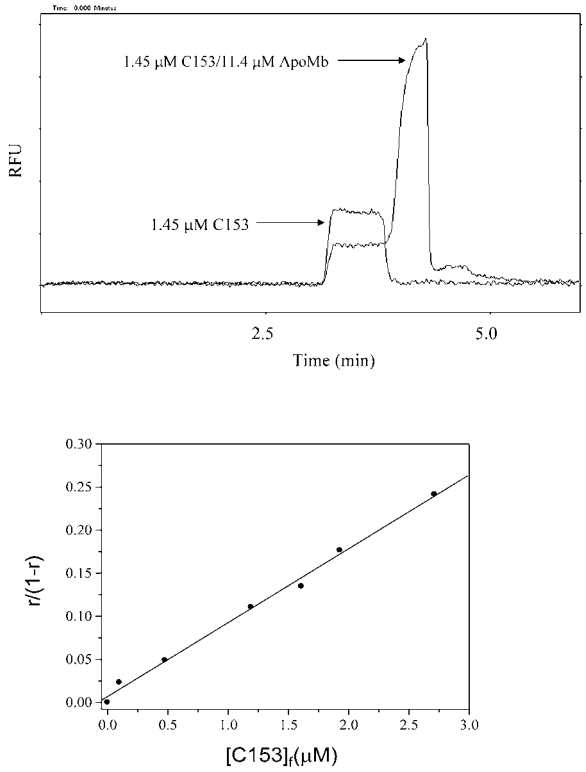

Figure 4. Electropherogram (top panel) obtained using the frontal analysis CE method with coumarin–ApoMb. Experimental conditions: pressure injection at 0.5 psi for 40 s; separation voltage, 10 kV; LIF detector with excitation at 488 nm and emission at 520 nm. Sodium-phosphate buffer (0.2 *M*) at pH 9.0. The first peak plateau is due to the coumarin and the second, to the coumarin–ApoMb complex. The final result is based on three individual experiments: K_D = 13 ± 2 μ*M*. The ordinate label RFU stands for relative fluorescence units. The bottom panel is a plot of {r/(1 − r)} against free coumarin, where r is the fraction of C153 bound per protein. The slope of a linear fit to the experimental data points gives the binding constant (K_B) of C153 in the complex. The value of K_B obtained from this figure is 0.086 μM^{-1}, which gives K_D = 11.6 μ*M*.

Using two different methods, we have obtained dissociation constants of 5.65 ± 0.25 μ*M* (Job's plot) and 13 ± 2 μ*M* (CE) for C153 and horse heart ApoMb, which are comparable with or smaller than those discussed previously for other fluorescent probes (29,30) (Figs. 3 and 4). The Job's plot of the complex (Fig. 3) clearly reveals that the maximum of the fluorescence intensity occurs at a coumarin mole fraction of 0.5, which is a clear indication of 1:1 stoichiometry for the complex in the given concentration range of protein. One explanation for the difference in the two results is that the CE experiments were performed using a higher C153–ApoMb ratio because the detector was equipped with a 488 nm light source, which is not optimal for exciting C153 fluorescence.

Independent confirmation that the coumarin binds in the heme pocket is provided by the similarity of the CD spectra of native myoglobin with those of the C153–ApoMb complex (Fig. 5). A comparison of the fluorescence anisotropy decay of C153 in solution (dimethyl sulfoxide [DMSO]) (Fig. 6) and that bound to ApoMb (Fig. 7) also argues for C153–ApoMb complex formation.

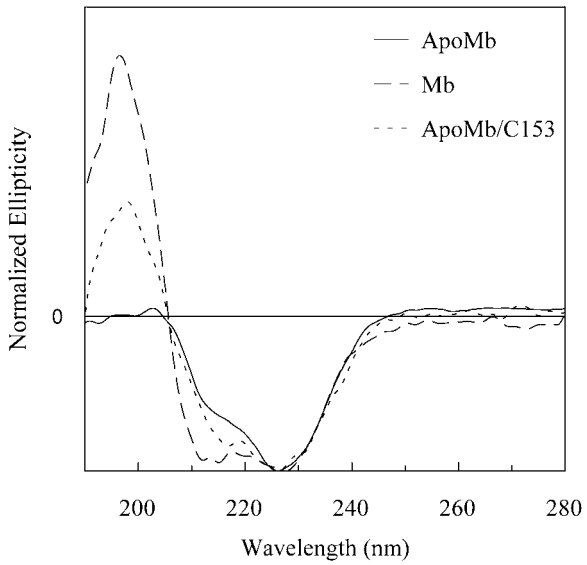

Figure 5. The CD spectra of ApoMb (solid), Mb (dashed) and ApoMb–C153 complex (dotted). The figure clearly shows the retention of the native structure of Mb once C153 binds inside the vacant heme pocket of ApoMb. Protein concentrations are approximately 10^{-6} *M*, and the ApoMb–C153 complex has a concentration ratio of 2:1. Similar spectra were obtained with other ratios in a range from 9:1 to 2:1.

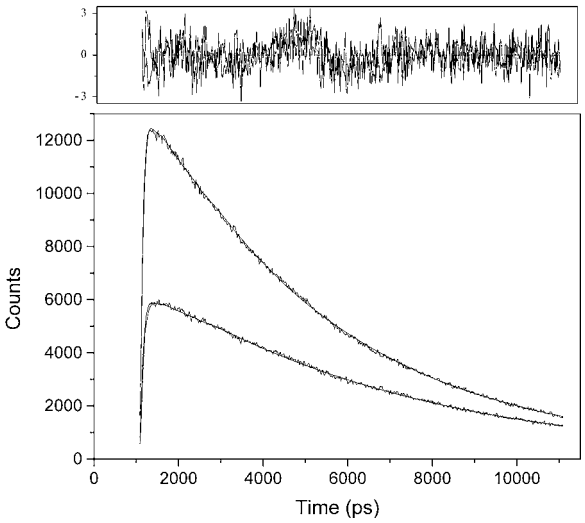

Figure 7. Polarized fluorescence decay of the C153–horse heart ApoMb complex. The concentration of protein (5.5×10^{-5} *M*) is 10 times that of coumarin to eliminate multiple binding of C153 to the protein. λ_{ex} = 425 nm; $\lambda_{em} > 550$ nm, $\chi^2 = 1.2$; r(t) = 0.29 exp(–t/9300 ps). The anisotropy measurement was repeated three times. The average value of rotational time is 9200 ± 100 ps, and the limiting anisotropy is r(0) = 0.29 ± 0.01. The fluorescence lifetime of coumarin bound to ApoMb was 5050 ± 50 ps (three measurements). For the lifetime measurements, λ_{ex} = 425 nm, $\lambda_{em} >$ 550 nm and $\chi^2 = 1.2$. Fitting the decay to a double exponential gave no improvement over the chi-squared value already obtained from the single-exponential fit. The top panel shows the residuals from the fits.

Although the free coumarin exhibits a very fast depolarization time of 100 ps in DMSO, this time is lengthened to 9.2 ns upon binding, the latter time consistent with the rotational correlation time that would be expected for the ~18 kDa protein. More significantly, the anisotropy decay of bound coumarin is single exponential (9.2 ns) within our time resolution. This can be interpreted in terms of a rigidly bound coumarin whose fluorescence is depolarized exclusively by the overall rotational motion of the ApoMb itself. A single-exponential decay would not be expected for a surface-bound chromophore (59,60). That the fluorescence decay of C153 is single exponential also suggests that, within the sensitivity of our experimental apparatus, it binds in the heme pocket in only one conformation.

Finally, there is a significant Stokes shift of bound C153 with respect to C153 in methanol that demonstrates the difference between the heme pocket and the bulk solvent in solvating the fluorescent state. The spectra in Fig. 8 can be used to compute

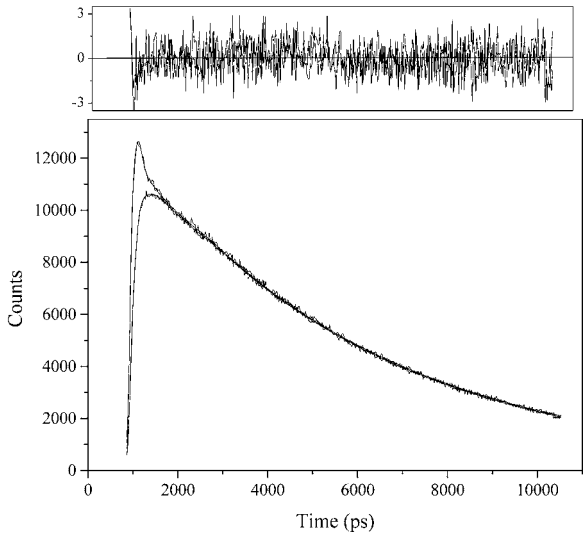

Figure 6. Polarized fluorescence decay of C153 in DMSO: λ_{ex} = 420 nm; $\lambda_{em} > 470$ nm, $\chi^2 = 1.3$; r(t) = 0.32 exp(–t/110 ps). The anisotropy measurement was repeated four times, yielding a reorientation time τ_r = 100 ± 10 ps and a limiting anisotropy r(0) = 0.32 ± 0.02. The fluorescence lifetime was 5300 ± 50 ps. The top panel shows the residual from the fits.

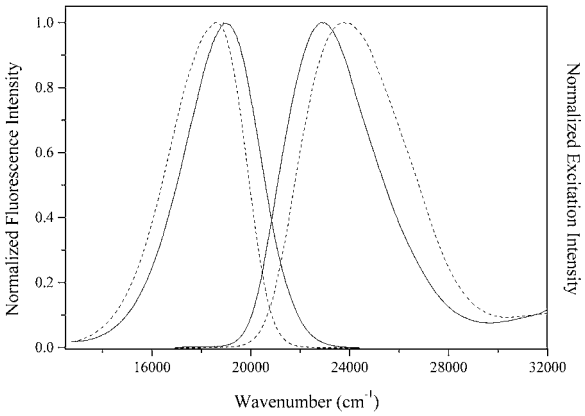

Figure 8. Steady-state spectra of the horse heart ApoMb–C153 complex (solid lines) and of C153 in methanol (dashed lines). According to our method of evaluating the reorganization energy (33), the whole excitation or absorption spectrum is needed. If there is more than one electronic excited state close to the fluorescence state, it will be very difficult to get an accurate excitation spectrum of that state, which is the case, for example, for ANS, whose excitation spectrum is congested with at least two overlapping peaks in the blue region. The reorganization energy calculated by our method for C153 in the complex was 2280 cm^{-1}, whereas that for C153 in methanol was 2800 cm^{-1}.

the reorganization energy, λ, using the method of Jordanides *et al*. (33):

$$\lambda = \hbar \frac{\int_0^\infty d\varpi[\sigma_a(\varpi) - \sigma_f(\varpi)]\varpi}{\int_0^\infty d\varpi[\sigma_a(\varpi) + \sigma_f(\varpi)]}$$

The σ_{af} are the absorption (or excitation) and emission spectra, respectively, on a wavenumber scale. The reorganization energy is widely used as a measure of the strength of interactions between a chromophore and its surrounding dielectric media in solvation dynamics studies. It is usually taken as half of the Stokes shift. This estimation is accurate if the excitation and emission spectra are Gaussian, but it becomes unreliable if the spectra are not Gaussian. The reorganization energy computed using the above expression is 2280 cm^{-1} for C153 complexed with ApoMb as opposed to 2800 cm^{-1} for C153 in methanol, which indicates the difference in the probe's environment in these two distinctly different systems.

The preponderance of evidence listed above supports C153 binding to ApoMb, specifically in the heme pocket, in a manner illustrated in Fig. 2. This leaves the dye in a hydrophobic environment consisting of a large number of amino acid side chains that are responsible for stabilizing and isolating the heme prosthetic group to prevent dissociation and oxidation in the native protein. In sperm whale myoglobin the principal side chains impinging on C153 are two His residues (at positions 64 and 97 in the primary sequence), Phe43, Val68, Leu29 and Leu89.

CONCLUSIONS

We have furnished an exhaustive characterization of the complex of the fluorescent probe C153 with ApoMb, indicating that it binds moderately strongly and very rigidly in the heme pocket. Because protein is clearly a heterogeneous environment with a spatially dependent polarizability, a precise knowledge of where and how the fluorescence probe binds is crucial to any thorough analysis of the protein dielectric response and our ability to distinguish the protein's response from that of the solvent. Future work will analyze the contribution of the individual amino acid residues in the heme pocket to the dielectric response of the protein.

Acknowledgements—This work was partially supported by NSF grant MCB-0077890 to M.S.H. and J.W.P. X.S. acknowledges the financial support provided by a grant from the Petroleum Research Fund, administered by the American Chemical Society. Mr. J. Graboski assisted with the preparation of the ApoMb samples. We thank Conoptics, Inc. for their generous loan of the Pockels cell to reduce the repetition rate of our Ti–sapphire system. We also thank Tijana Grove for assisting us with the CD measurements.

REFERENCES

1. Simon, J. D. (1988) Time-resolved studies of solvation in polar media. *Acc. Chem. Res.* **21**, 128.
2. Bagchi, B., A. Chandra and G. R. Fleming (1990) Dynamic solvent effects in adiabatic electron-transfer reactions—role of translational modes. *J. Phys. Chem.* **94**, 5197–5200.
3. Maroncelli, M. (1993) The dynamics of solvation in polar liquids. *J. Mol. Liq.* **57**, 1–37.
4. Hynes, J. T. (1994) Charge transfer reactions and solvation dynamics. In *Ultrafast Dynamics of Chemical Systems*, Vol. 7, (Edited by D.G. Truhlar) pp. 345–381. Kluwer Academic Publishers, Boston.
5. Stratt, R. M. and M. Maroncelli (1996) Nonreactive dynamics in solution: the emerging molecular view of solvation dynamics and vibrational relaxation. *J. Phys. Chem.* **100**, 12981–12996.
6. Fleming, G. R. and M. Cho (1996) Chromophore-solvent dynamics. *Ann. Rev. Phys. Chem.* **47**, 109–134.
7. DeBoeij, W. P., M. S. Pshenichnikov and D. A. Wiersma (1998) Ultrafast solvation dynamics explored by femtosecond photon echo spectroscopies. *Ann. Rev. Phys. Chem.* **49**, 99–123.
8. Mukamel, S. (1995) *Principles of Nonlinear Optical Spectroscopy*. Oxford University Press, New York.
9. Song, X. (1999) Theoretical studies of dielectric solvation dynamics. In *Treatment of Electrostatic Interactions in Computer Simulations of Condensed Media*, Vol. 492 (Edited by G. Hummer and L. R. Pratt), pp. 417–428. American Institute of Physics, New York.
10. Bhattacharyya, K. and B. Bagchi (2000) Slow dynamics of constrained water in complex geometries. *J. Phys. Chem. A* **104**, 10603–10613.
11. Hsu, C. P., X. Y. Song and R. A. Marcus (1997) Time-dependent Stokes shift and its calculation from solvent dielectric dispersion data. *J. Phys. Chem. B* **101**, 2546–2551.
12. Song, X. and D. Chandler (1998) Dielectric solvation dynamics of molecules of arbitrary shape and charge distribution. *J. Chem. Phys.* **108**, 2594–2600.
13. Lang, M. J., X. J. Jordanides, X. Song and G. R. Fleming (1999) Aqueous solvation dynamics studied by photon echo spectroscopy. *J. Chem. Phys.* **110**, 5884–5892.
14. Marcus, R. A. and N. Sutin (1985) Electron transfers in chemistry and biology. *Biochim. Biophys. Acta* **811**, 265–322.
15. King, G. and A. Warshel (1990) Investigation of the free energy functions for electron transfer reactions. *J. Chem. Phys.* **91**, 3647.
16. Bader, J. S., R. A. Kuharski and D. Chandler (1990) Role of nuclear tunneling in aqueous ferrous ferric electron-transfer. *J. Chem. Phys.* **93**, 230–236.
17. Zheng, C., C. F. Wong, J. A. McCammon and P. G. Wolynes (1989) Classical and quantum aspects of ferrocytochrome c. *Chem. Scr.* **29A**, 171–179.
18. Simonson, T. (2002) Gaussian fluctuations and linear response in an electron transfer protein. *Proc. Natl. Acad. Sci. USA* **99**, 6544–6549.
19. Warshel, A. and S. T. Russel (1984) Calculation of electrostatic interactions in biological systems and in solutions. *Q. Rev. Biophys.* **17**, 283–422.
20. Sharp, K. A. and B. Honig (1990) Electrostatic interactions in macromolecules: theory and applications. *Ann. Rev. Biophys. Chem.* **19**, 301–332.
21. Schutz, C. N. and A. Warshel (2001) What are the dielectric ''constants'' of proteins and how to validate electrostatic models? *Proteins Struct. Funct. Genet.* **44**, 400–417.
22. Simonson, T. (2001) Macromolecular electrostatics: continuum models and their growing pains. *Curr. Opin. Struct. Biol.* **11**, 243–252.
23. Nakamura, H. (1996) Roles of electrostatic interaction in proteins. *Q. Rev. Biophys.* **29**, 1–90.
24. Brooks, C. L., M. Karplus and B. M. Pettitt (1987) Proteins: a theoretical perspective of dynamics, structure, and thermodynamics. *Adv. Chem. Phys.* **71**, 259–320.
25. Sheppard, R. J., E. H. Grant and G. P. South (1978) *Dielectric Behavior of Biological Molecules*, 1st ed. Oxford University Press, Clarendon.
26. Pethig, R. (1992) Protein-water interactions determined by dielectric methods. *Ann. Rev. Phys. Chem.* **43**, 177–205.
27. Pal, S. K., J. Peon, B. Bagchi and A. H. Zewail (2002) Biological water: femtosecond dynamics of macromolecular hydration. *J. Phys. Chem. B* **106**, 12376–12395.
28. Nandi, N., K. Bhattacharyya and B. Bagchi (2000) Dielectric relaxation and solvation dynamics of water in complex chemical and biological systems. *Chem. Rev.* **100**, 2013–2045.
29. Pierce, D. W. and S. G. Boxer (1992) Dielectric-relaxation in a protein matrix. *J. Phys. Chem.* **96**, 5560–5566.
30. Bashkin, J. S., G. Mclendon, S. Mukamel and J. Marohn (1990) Influence of medium dynamics on solvation and charge separation reactions—comparison of a simple alcohol and a protein solvent. *J. Phys. Chem.* **94**, 4757–4761.
31. Homoelle, B. J., M. D. Edington W. M. Diffey and W. F. Beck (1998) Stimulated photon-echo and transient-grating studies of protein-matrix solvation dynamics and interexciton-state radiationless decay in phycocyanin and allopycocyanin. *J. Phys. Chem. B* **102**, 3044–3052.
32. Fraga, E. and G. R. Loppnow (1998) Proteins as solvents: blue copper proteins as a molecular ruler for solvent effects on resonance Raman intensities. *J. Phys. Chem. B* **102**, 7659–7665.

33. Jordanides, X. J., M. J. Lang, X. Y. Song and G. R. Fleming (1999) Solvation dynamics in protein environments studied by photon echo spectroscopy. *J. Phys. Chem. B* **103**, 7995–8005.
34. Pal, S. K., J. Peon and A. H. Zewail (2002) Biological water at the protein surface: dynamical solvation probed directly with femtosecond resolution. *Proc. Natl. Acad. Sci. USA* **99**, 1763–1768.
35. Peon, J., S. K. Pal and A. H. Zewail (2002) Hydration at the surface of the protein Monellin: dynamics with femtosecond resolution. *Proc. Natl. Acad. Sci. USA* **99**, 10964–10969.
36. Maroncelli, M. and G. R. Fleming (1987) Picosecond solvation dynamics of coumarin-153—the importance of molecular aspects of solvation. *J. Chem. Phys.* **86**, 6221–6239.
37. Horng, M. L., J. Gardecki, A. Papazyan and M. Maroncelli (1995) Subpicosecond measurements of polar solvation dynamics: coumarin 153 revisited. *J. Phys. Chem.* **99**, 17311–17337.
38. Lewis, J. E. and M. Maroncelli (1998) On the (uninteresting) dependence of the absorption and emission transition moments of coumarin 153 on solvent. *Chem. Phys. Lett.* **282**, 197–203.
39. Kovalenko, S. A., J. Ruthmann and N. P. Ernsting (1997) Ultrafast Stokes shift and excited-state transient absorption of coumarin 153 in solution. *Chem. Phys. Lett.* **271**, 40–50.
40. Muhlpfordt, A., R. Schanz, N. P. Ernsting, V. Farztdinov and S. Grimme (1999) Coumarin 153 in the gas phase: optical spectra and quantum chemical calculations. *Phys. Chem. Chem. Phys.* **1**, 3209–3218.
41. Changenet-Barret, P., C. T. Choma, E. F. Gooding, W. F. DeGrado and R. M. Hochstrasser (2000) Ultrafast dielectric response of proteins from dynamic Stokes shifting of coumarin in calmodulin. *J. Phys. Chem. B* **104**, 9322–9329.
42. Jiang, Y., P. K. McCarthy and D. J. Blanchard (1994) The role of multiple electronic states in the dissipative energy dynamics of coumarin 153. *Chem. Phys.* **183**, 249–267.
43. Flory, W. C. and D. J. Blanchard (1998) Excitation energy-dependent transient spectral relaxation of coumarin 153. *Appl. Spectrosc.* **52**, 82–90.
44. Palmer, P. M., Y. Chen and M. R. Topp (2000) Simple water clusters of coumarins 151 and 152A studied by IR-UV double resonance spectroscopy. *Chem. Phys. Lett.* **318**, 440–447.
45. Chen, Y., P. M. Palmer and M. R. Topp (2002) Infrared spectroscopy of jet-cooled, electronically excited clusters of coumarin 151: excited-state interactions and conformational relaxation. *Int. J. Mass Spectrom.* **220**, 231–251.
46. Agmon, N. (1990) Dynamic stokes shift in coumarin: is it only relaxation? *J. Phys. Chem.* **94**, 2959–2963.
47. Kundu, S., B. Snyder, K. Das, P. K. Chowdhury, J. Park, J. W. Petrich and M. S. Hargrove (2002) The leghemoglobin proximal heme pocket directs oxygen dissociation and stabilizes bound heme. *Proteins Struct. Funct. Genet.* **46**, 268–277.
48. Kundu, S. and M. S. Hargrove (2003) Distal heme pocket regulation of ligand binding and stability in soybean leghemoglobin. *Proteins Struct. Funct. Genet.* **50**, 239–248.
49. Quillin, M. L., R. M. Arduini, J. S. Olson and G. N. Phillips Jr. (1993) High-resolution crystal structures of distal histidine mutants of sperm whale myoglobin. *J. Mol. Biol.* **234**, 140–155.
50. Quillin, M. L., T. Li, J. S. Olson, G. N. Phillips Jr., Y. Dou, M. Ikeda-Saito, R. Regan, M. Carlson, Q. H. Gibson and H. Li (1995) Structural and functional effects of apolar mutations of the distal valine in myoglobin. *J. Mol. Biol.* **245**, 416–436.
51. Cocco, M. J. and J. T. J. Lecomte (1994) The native state of apomyoglobin described by proton NMR spectroscopy: interaction with the paramagnetic probe HyTEMPO and the fluorescent dye ANS. *Protein Sci.* **3**, 267–281.
52. Wagner, U. G., N. Muller, W. Schmitzberger, H. Falk and C. Kratky (1995) Structure determination of the biliverdin apomyoglobin complex—crystal-structure analysis of 2 crystal forms at 1.4 and 1.5 Angstrom resolution. *J. Mol. Biol.* **247**, 326–337.
53. Shen, X. and J. R. Knutson (2001) Subpicosecond fluorescence spectra of tryptophan in water. *J. Phys. Chem. B* **105**, 6260–6265.
54. Hargrove, M. S., E. W. Singleton, M. L. Quillin, L. A. Ortiz, G. N. Phillips, J. S. Olson and A. J. Mathews (1994) His(64)(E7)→Tyr apomyoglobin as a reagent for measuring rates of hemin dissociation. *J. Biol. Chem.* **269**, 4207–4214.
55. Williams, K. R., B. Adhyaru, R. Pierce and S. G. Schulman (2002) The binding constant of complexation of bilrubin to bovine serum albumin. *J. Chem. Educ.* **79**, 115–116.
56. Procacci, P., T. A. Darden, E. Paci and M. Massimo (1997) ORAC: a molecular dynamics program to simulate complex molecular systems with realistic electrostatic interactions. *J. Comput. Chem.* **18**, 1848–1862.
57. Tuckerman, M. E., B. Berne and G. J. Martyna (1992) Reversible multiple scale molecular dynamics. *J. Chem. Phys.* **97**, 1990–2001.
58. Marchi, M. and P. Procacci (1998) Coordinate scaling and multiple time step algorithms for simulation of solvated proteins in the NPT ensemble. *J. Chem. Phys.* **109**, 5194–5202.
59. Petrich, J. W., J. W. Longworth and G. R. Fleming (1987) Internal motion and electron transfer in proteins: a picosecond fluorescence study of three homologous azurins. *Biochemistry* **26**, 2711–2722.
60. Das, K., A. V. Smirnov, J. Wen, P. Miskovsky and J. W. Petrich (1999) Photophysics of hypericin and hypocrellin A in complex with subcellular components: interactions with human serum albumin. *Photochem. Photobiol.* **69**, 633–645.